

Electronic supplementary information

**A Five-Carbon Unsaturated Criegee Intermediate: Synthesis, Spectroscopic Identification, and Theoretical Study of 3-penten-2-one oxide**

Tarun Kumar Roy<sup>†</sup>, Tianlin Liu<sup>†</sup>, Yujie Qian, Christopher Sojda, Marisa Kozlowski,  
and Marsha I. Lester\*

Department of Chemistry, University of Pennsylvania, Philadelphia, PA 19104-6323 USA

<sup>†</sup> Equal contributions.

\*Corresponding author email: [milester@sas.upenn.edu](mailto:milester@sas.upenn.edu)

---

## Table of Contents

S1. Synthesis of (Z)-2,4-diiodopent-2-ene precursor .....	S3
S1.1. General Methods .....	S3
S1.2. Synthesis Procedures.....	S3
Figure S1. <sup>1</sup> H NMR of pent-3-yn-2-ol.....	S7
Figure S2. <sup>13</sup> C NMR of pent-3-yn-2-ol .....	S7
Figure S3. <sup>1</sup> H NMR of (Z)-4-iodopent-3-en-2-ol.....	S8
Figure S4. <sup>13</sup> C NMR of (Z)-4-iodopent-3-en-2-ol.....	S8
Figure S5. <sup>1</sup> H NMR of (Z)-2,4-diiodopent-2-ene.....	S9
Figure S6. <sup>13</sup> C NMR of (Z)-2,4-diiodopent-2-ene.....	S9
S2. Experimental Methods .....	S10
S3. Theoretical Methods.....	S11
Scheme S1. Alkene Ozonolysis of 2-methylpenta-1,3-diene .....	S13
S4. Unimolecular Reaction Pathways and Potential Isomers.....	S14
Scheme S2. 1,4 H-atom Transfer Mechanism.....	S14
Scheme S3. 1,6 H-atom Transfer Mechanism.....	S15
Scheme S4. 1,5 Ring-Closure Mechanism .....	S15
S5. Supplementary Experimental Results .....	S16
Figure S7. Full Mass Spectra with and without Precursor Photolysis .....	S16
Figure S8. Power Dependence for OPO-Induced Ground-State Depletion .....	S17
S6. Supplementary Theoretical Results.....	S18
Figure S9. Conformers of 3-penten-2-one oxide.....	S18
Figure S10. Molecular Orbitals of <i>tEE</i> Conformer .....	S19
S6.1. Additional Simulated Absorption Spectra.....	S20
Figure S11. Simulated Absorption Spectra for Low-Energy Conformers of 5C CI .....	S21
Table S1. <i>cis-trans</i> Isomerization Barriers.....	S22
Table S2. 1,4 and 1,6 H-atom Transfer Transition State Barriers .....	S23
Table S3. Calculated Ionization Energies of 5C CI Conformers .....	S24
Table S4. Calculated Ionization and Vertical Excitation Energies of Potential Isomers of 5C CI .....	S25
Table S5. Simulated Absorption Maxima and Associated Cross-Sections of 5C CI Conformers.....	S26
Table S6. Optimized Geometries of 5C CI Conformers .....	S27

## S1. Synthesis of (Z)-2,4-diiodopent-2-ene precursor

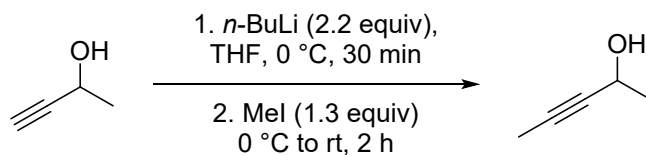
### S1.1. General Methods

All reactions were performed under an argon atmosphere unless otherwise noted with oven-dried glassware using standard Schlenk or vacuum line techniques. Reaction flasks were covered with aluminum foil and workups were performed with the lights off to limit light degradation. All reactions mixtures were stirred using RCT Digital IKA Magnetic Stirrer Plates. Dry  $\text{CH}_2\text{Cl}_2$  was obtained by freshly distilling from  $\text{CaH}_2$  under an atmosphere of argon. Dry and degassed THF was obtained using a solvent purification system. Commercially available reagents were obtained from Sigma-Aldrich, TCI America, or Acros Organics, and solvents were obtained from Fisher Scientific. Analytical thin-layer chromatography (TLC) was used to monitor reaction progress and was performed using Silicycle 250  $\mu\text{m}$  precoated 60 Å silica gel plates with F254 indicator using shortwave ultraviolet light to visualize, or potassium permanganate stain. Purification via flash chromatography was done using 230 – 400 mesh silica gel obtained from Silicycle.  $^1\text{H}$  NMR spectra were obtained using a 400 MHz spectrometer. Decoupled  $^{13}\text{C}\{^1\text{H}\}$  NMR spectra were recorded at 101 MHz. Chemical shifts are reported in parts per million (ppm) from the solvent resonance,  $\text{CDCl}_3$  7.26 ppm  $^1\text{H}$  NMR, and  $\text{CDCl}_3$  77.16 ppm, for  $^{13}\text{C}$  NMR. Data are reported as follows: chemical shift, multiplicity (s = singlet, d = doublet, t = triplet, m = multiplet, tt = triplet of triplets, dq = doublet of quartets, br = broad), coupling constants, and number or protons. Deuterated solvents were obtained from Cambridge Isotope Laboratories, Inc. Infrared (IR) absorption spectra were taken on a FT-IR spectrometer (ATR, neat). Accurate mass measurement analyses were conducted on either a GCMS with electron ionization (EI) or an LCMS with electrospray ionization (ESI). The signals were mass measured (TOF) against an internal lock mass reference of perfluorotriethylamine (PFTBA) for EI-GCMS, and leucine enkephalin for ESI-LCMS. Waters software calibrates the instruments, and reports measurements, by use of neutral atomic masses; the mass of the electron is not subtracted (positive ions) or added (negative ions).

### S1.2. Synthesis Procedures

**Caution:** Special care should be taken in handling alkylating agents, especially low molecular weight alkylating agents, due to their carcinogenic properties. Excess alkylating agents should be destroyed using a large excess of water, or sodium hydroxide.

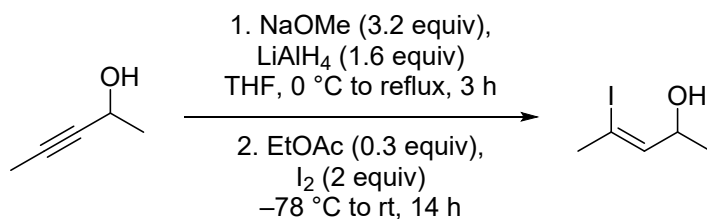
**Caution:** n-Butyllithium is extremely reactive and potentially pyrophoric. Uncontrolled exposure of the reagent to protic solvents or moisture may result in a fire. Safe handling using glass syringes under Ar is required and the reagent can be quenched by the slow addition of water or satd  $\text{NH}_4\text{Cl}$  with cooling.



**Pent-3-yn-2-ol.** To a dry 1 L 3-neck flask was added but-3-yn-2-ol (10.0 mL, 128 mmol) followed by dry THF (220 mL). An oven-dried addition funnel was attached and the solution was cooled to 0 °C and purged with Ar. *n*-Butyllithium (2.5 M hexane, 112 mL, 281 mmol) was added dropwise over the course of 10 min via the the addition funnel. After the addition, the mixture was left stirring for 20 min at 0 °C before adding MeI (10.3 mL, 166 mmol) over the course of ~1 min and the solution was removed from the ice bath and allowed to warm to room temperature over the course of 2 h. The solution was cooled back to 0 °C and 1 M NaOH (50 mL) was added. After stirring for 10 min, the solution was further diluted with deionized water (500 mL) and extracted with Et<sub>2</sub>O (3 x 100 mL). The organic washings were combined, washed with saturated NaCl (75 mL), dried with anhydrous MgSO<sub>4</sub>, filtered, and concentrated to yield an orange oil. The material was purified by distillation at reduced pressure (42 °C, 9 Torr) to yield pent-3-yn-2-ol as a clear liquid (5.09 g, 47%). Impure fractions were saved and added to future batches. The NMR spectra are consistent with those reported in literature.<sup>1</sup>

<sup>1</sup>H NMR (400 MHz, CDCl<sub>3</sub>) δ 4.49 (tt, *J* = 6.7, 2.0 Hz, 1H), 1.84 (d, *J* = 2.1 Hz, 3H), 1.77 (br, 1H), 1.42 (d, *J* = 6.6 Hz, 3H).

<sup>13</sup>C NMR (101 MHz, CDCl<sub>3</sub>) δ 81.5, 80.3, 58.7, 24.8, 3.6.



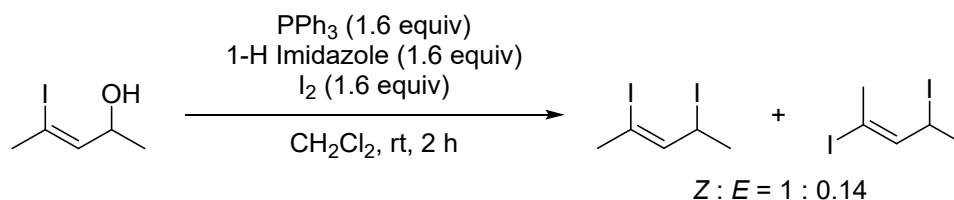
**(Z)-4-Iodopent-3-en-2-ol.** This compound was prepared using an established literature procedure.<sup>2</sup> To a dry 250 mL round bottom flask was added NaOMe (1.45 g, 26.8 mmol) followed by LiAlH<sub>4</sub> (0.508 g, 13.4 mmol). The flask was purged with Ar, cooled to 0 °C, and dry THF (29 mL) was added. A solution of pent-3-yn-2-ol (0.704 g, 8.37 mmol) in dry THF (14 mL) was added to the reaction mixture over the course of ~5 min via cannula transfer and the mixture was heated to reflux. After 3 h, the mixture was cooled to -78 °C and dry EtOAc (0.25 mL, 2.6 mmol) was added. After 10 min of stirring, a solution of I<sub>2</sub> (4.25 g, 16.7 mmol) in dry THF (25 mL) was added via cannula transfer over the course of ~20 min and the mixture was left to warm to room temperature in the dry ice bath overnight. After 14 h, the mixture was cooled to 0 °C, diluted with dry Et<sub>2</sub>O (50 mL), and quenched by slow addition of deionized water (0.5 mL), 15% NaOH (0.5 mL), and a second addition of deionized water (1.5 mL) at which point the mixture

was removed from the ice bath and left to stir for 20 min. Anhydrous MgSO<sub>4</sub> was added to the mixture and the slurry was allowed to stir for 20 min before filtering and washing the solid with Et<sub>2</sub>O. The filtrate was diluted with deionized water (150 mL) and washed with Et<sub>2</sub>O (3 x 50 mL). The organic washings were combined, washed with saturated NaCl (50 mL), dried with anhydrous MgSO<sub>4</sub>, filtered, and concentrated. The resultant material was purified via column chromatography using 10-20% EtOAc in hexanes to yield 4-iodopent-3-en-2-ol as a pale-yellow oil (1.144 g, 64%). The NMR spectra are consistent with those reported in literature.<sup>3</sup>

<sup>1</sup>H NMR (400 MHz, CDCl<sub>3</sub>) δ 5.54 (dq, *J* = 7.4, 1.5 Hz, 1H), 4.47 – 4.34 (m, 1H), 2.51 (d, *J* = 1.5 Hz, 3H), 1.74 (d, *J* = 3.0 Hz, 1H), 1.28 (d, *J* = 6.4 Hz, 3H).

<sup>13</sup>C NMR (101 MHz, CDCl<sub>3</sub>) δ 139.0, 100.8, 73.2, 33.8, 22.1.

**Caution:** Special care should be taken in handling alkylating agents, especially low molecular weight alkylating agents, due to their carcinogenic properties. The **product** is likely a strong alkylating agent and should be handled with care.



**(Z)-2,4-Diiodopent-2-ene.** Triphenylphosphine (2.264 g, 8.63 mmol), iodine (2.191 g, 8.63 mmol), and 1H-imidazole (0.588 g, 8.63 mmol) were added to a dry 200 mL round-bottom flask. The flask was covered with aluminum foil and purged with Ar and dry CH<sub>2</sub>Cl<sub>2</sub> (42 mL) was added to the flask. After 20 min of vigorous stirring, (Z)-4-iodo-3-en-2-ol (1.144 g, 5.39 mmol) dissolved in dry CH<sub>2</sub>Cl<sub>2</sub> (21 mL) was added to the reaction mixture via syringe over the course of ~5 min. The reaction was complete as determined by TLC after 2 h at which time the reaction mixture was poured into ice-cold Et<sub>2</sub>O (200 mL) and the precipitated solid was filtered and washed with additional ice-cold Et<sub>2</sub>O (25 mL). The combined organic fractions were concentrated and filtered through a pad of neutral alumina using hexanes to elute the product (~100 mL). The filtrate was washed with saturated NaHSO<sub>3</sub> (2 x 25 mL), saturated NaCl (25 mL), dried with anhydrous MgSO<sub>4</sub>, filtered, and concentrated to yield pure 2,4-diiodopent-2-ene (1:0.14 Z:E) as a pink oil (0.846 g, 2.63 mmol 49%). Pure material was segregated into multiple small vials, stabilized with copper pellets (approx. 0.1 - 0.2 g), purged with argon, and stored at -20 °C to mitigate decomposition.

**<sup>1</sup>H NMR** (400 MHz, CDCl<sub>3</sub>)

**(Z)-2,4-diiodopent-2-ene:** δ 5.76 (dq, *J* = 10.0, 1.5, 1.5, 1.5 Hz, 1H), 4.86 (dq, *J* = 10.0, 6.7, 6.7, 6.7 Hz, 1H), 2.49 (d, *J* = 1.5 Hz, 3H), 1.96 (d, *J* = 6.8 Hz, 3H).

**(E)-2,4-diiodopent-2-ene:** δ 6.49 (dq, *J* = 10.9, 1.5, 1.4, 1.4 Hz, 1H), 4.95 (dq, *J* = 10.9, 6.8, 6.7, 6.7 Hz, 1H), 2.36 (d, *J* = 1.6 Hz, 3H), 1.91 (d, *J* = 6.7 Hz, 3H).

**<sup>13</sup>C NMR** (101 MHz, CDCl<sub>3</sub>)

**(Z)-2,4-diiodopent-2-ene:** δ 139.9, 102.3, 33.4, 31.2, 28.1.

**(E)-2,4-diiodopent-2-ene:** δ 144.9, 96.8, 28.8, 27.8, 21.4.

**HRMS (ESI, TOF)** *m/z*: [M-H]<sup>-</sup> calculated for C<sub>5</sub>H<sub>7</sub>I<sub>2</sub> 320.8637, observed 320.8633.

**IR (film)** 2957, 2911, 1711, 1634, 1440, 1424, 1374, 1263, 1161, 1136, 837, 551 cm<sup>-1</sup>.

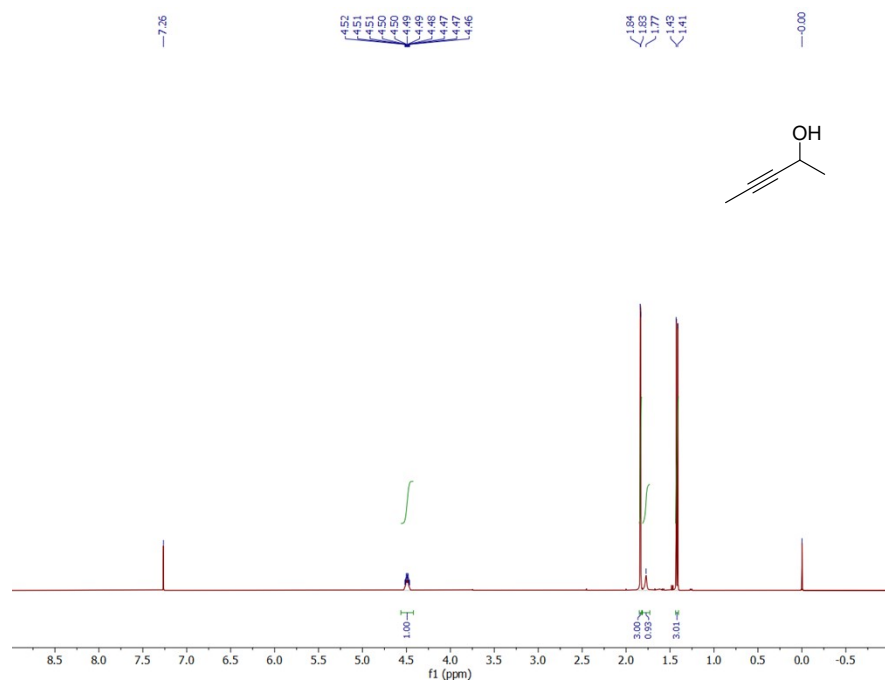


**Figure S1:** Pent-3-yn-2-ol:  $^1\text{H}$  NMR (400 MHz,  $\text{CDCl}_3$ )  $\delta$  4.49 (tt,  $J = 6.7, 2.0$  Hz, 1H), 1.84 (d,  $J = 2.1$  Hz, 3H), 1.77 (br, 1H), 1.42 (d,  $J = 6.6$  Hz, 3H).

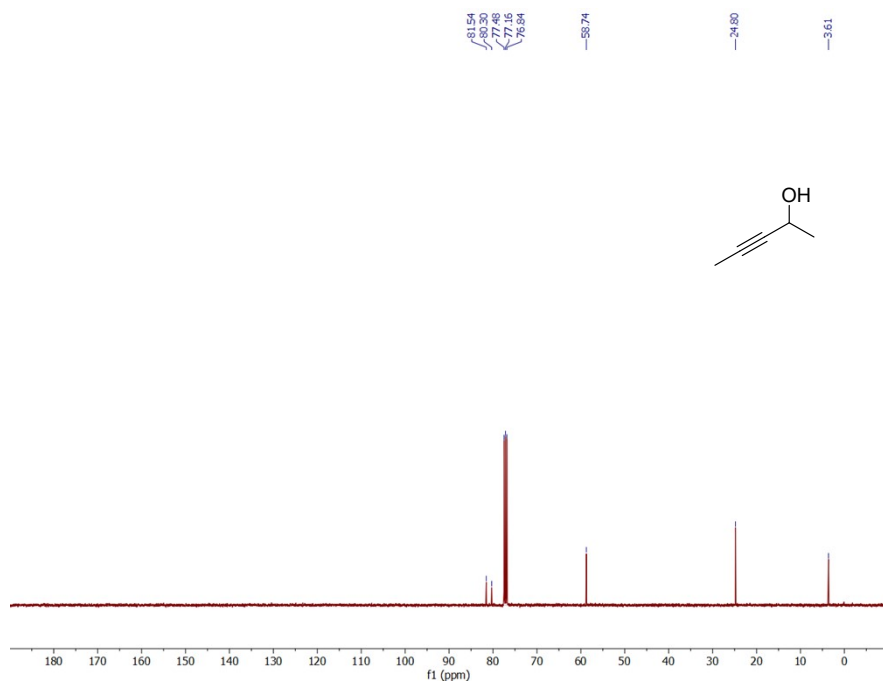


**Figure S2:** Pent-3-yn-2-ol:  $^{13}\text{C}$  NMR (101 MHz,  $\text{CDCl}_3$ )  $\delta$  81.5, 80.3, 58.7, 24.8, 3.6.

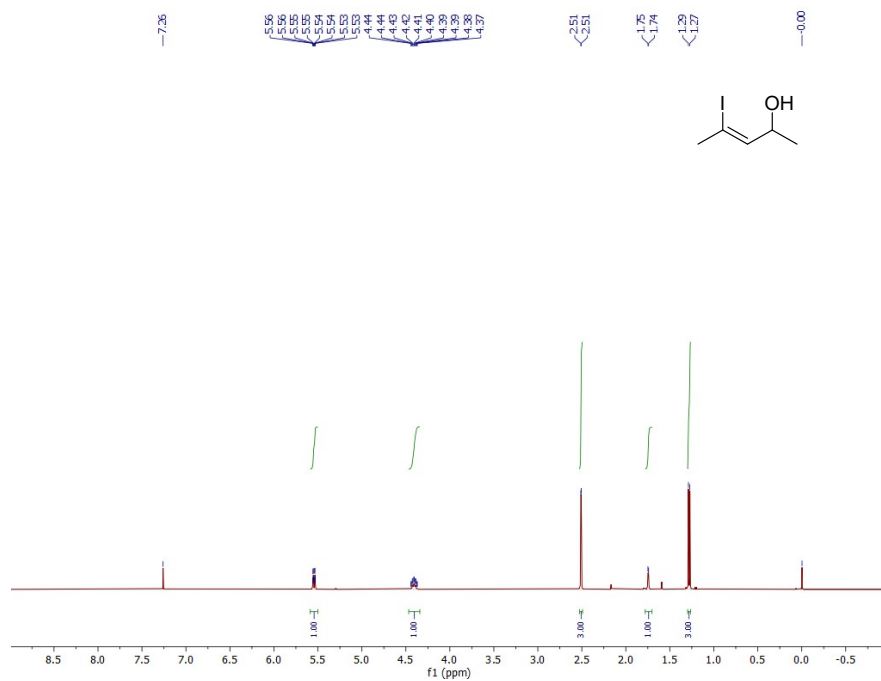


**Figure S3:** (Z)-4-Iodopent-3-en-2-ol:  $^1\text{H}$  NMR (400 MHz,  $\text{CDCl}_3$ )  $\delta$  5.54 (dq,  $J = 7.4, 1.5$  Hz, 1H), 4.47 – 4.34 (m, 1H), 2.51 (d,  $J = 1.5$  Hz, 3H), 1.74 (d,  $J = 3.0$  Hz, 1H), 1.28 (d,  $J = 6.4$  Hz, 3H).

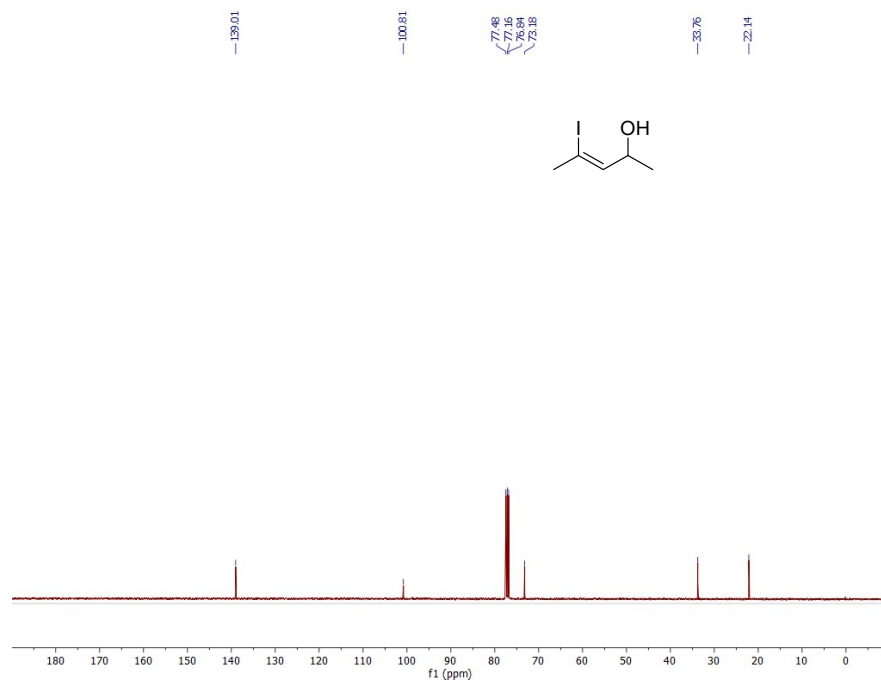


**Figure S4:** (Z)-4-Iodopent-3-en-2-ol:  $^{13}\text{C}$  NMR (101 MHz,  $\text{CDCl}_3$ )  $\delta$  139.0, 100.8, 73.2, 33.8, 22.1.

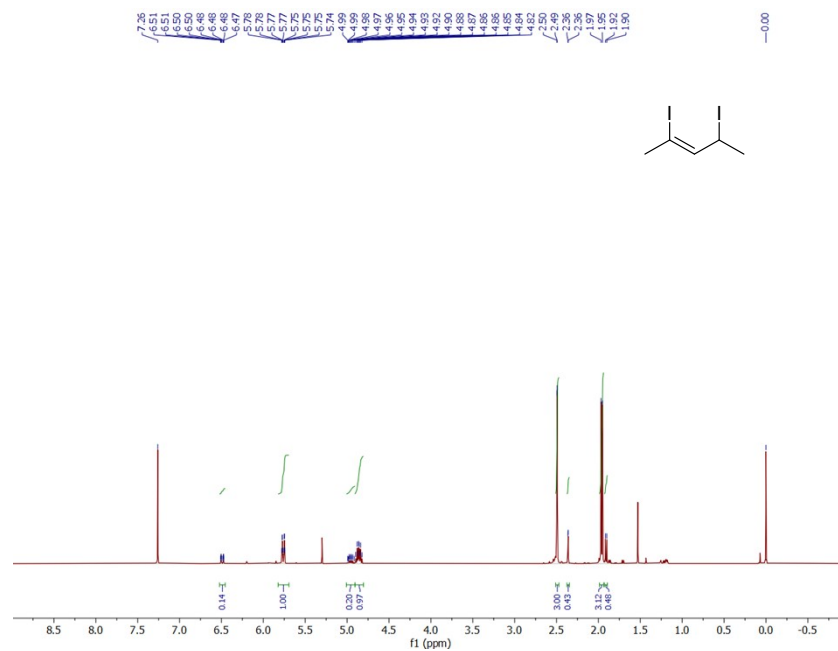


**Figure S5:**  $^1\text{H}$  NMR (400 MHz,  $\text{CDCl}_3$ ): (*Z*)-2,4-diiodopent-2-ene:  $\delta$  5.76 (dq,  $J = 10.0, 1.5, 1.5, 1.5$  Hz, 1H), 4.86 (dq,  $J = 10.0, 6.7, 6.7, 6.7$  Hz, 1H), 2.49 (d,  $J = 1.5$  Hz, 3H), 1.96 (d,  $J = 6.8$  Hz, 3H). (*E*)-2,4-diiodopent-2-ene:  $\delta$  6.49 (dq,  $J = 10.9, 1.5, 1.4, 1.4$  Hz, 1H), 4.95 (dq,  $J = 10.9, 6.8, 6.7, 6.7$  Hz, 1H), 2.36 (d,  $J = 1.6$  Hz, 3H), 1.91 (d,  $J = 6.7$  Hz, 3H).

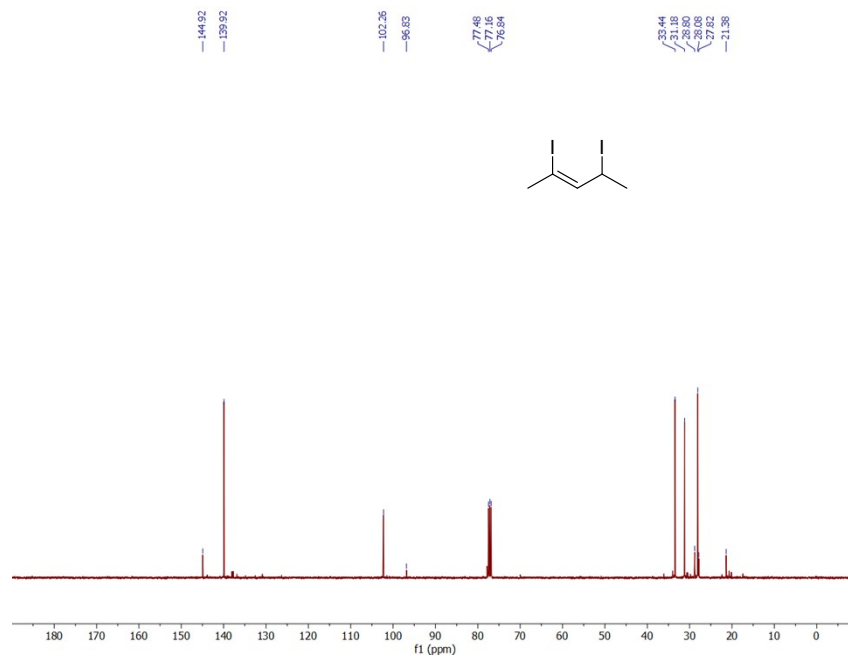


**Figure S6:**  $^{13}\text{C}$  NMR (101 MHz,  $\text{CDCl}_3$ ): (*Z*)-2,4-diiodopent-2-ene:  $\delta$  139.9, 102.3, 33.4, 31.2, 28.1. (*E*)-2,4-diiodopent-2-ene:  $\delta$  144.9, 96.8, 28.8, 27.8, 21.4.

## S2. Experimental Methods

The five-carbon unsaturated 3-penten-2-one oxide intermediates are generated in a quartz capillary reactor tube and cooled in a pulsed jet expansion. The experimental methods used to produce various CIs in this laboratory are available elsewhere.<sup>4-7</sup> Briefly, the (*Z*)-2,4-diiodopent-2-ene precursor is heated to 45°C using a Peltier thermoelectric heating module (Laird Technologies, PC4), and the temperature is monitored by a digital thermometer (Cole-Parmer, Type K). The vapor of the diiodoalkene precursor is seeded in a 20% O<sub>2</sub>/Ar carrier gas at 10 psi and pulsed through an affixed quartz capillary reactor tube (1 mm inner diameter; 25 mm length) into the vacuum chamber. The precursor is photolyzed near the exit of the capillary tube using cylindrically focused 248 nm output (~ 30 mJ/pulse, 10 Hz) of a KrF excimer laser (Coherent Compex 102). The resultant monoiodo radical reacts with O<sub>2</sub> to produce 3-penten-2-one oxide Criegee intermediates. The newly formed Criegee intermediates are collisionally stabilized in the capillary tube and cooled to a rotational temperature of ~ 10 K during the supersonic jet expansion.<sup>8</sup> The resultant 3-penten-2-one oxide CIs are characterized through two sets of experiments.

In the first set of experiments, the Criegee intermediates are detected 4.5 cm downstream in a collision-free region using a time-of-flight mass spectrometer (TOF-MS, RM Jordan). The intermediates are detected via photoionization using 118 nm (10.5 eV) vacuum ultraviolet (VUV) radiation on the parent *m/z* 100 mass channel. The fixed frequency VUV radiation at 118 nm is generated by frequency tripling the third harmonic of an Nd:YAG laser (Continuum Powerlite 9010) at 355 nm (~ 31 mJ/pulse, 10 Hz) in a phase-matched Xe:Ar gas mixture. The UV-vis depletion spectrum of the 3-penten-2-one oxide intermediates is recorded by monitoring the UV-vis induced depletion of the VUV photoionization signal at *m/z* 100. For depletion measurements, counter-propagating UV-vis radiation (5 Hz) is introduced ~50 ns prior to VUV photoionization. The focused UV-vis laser beam is spatially overlapped with the VUV beam in the interaction region of the TOF-MS. A broadly tunable BBO-OPO (EKSPLA 342NT, 3-5 ns pulse width, 5 cm<sup>-1</sup> linewidth) is used to produce UV-vis radiation. The sum frequency generation (SFG) of the 1064 nm Nd:YAG fundamental and OPO signal output is employed in the 325-405 nm spectral range, while the OPO signal output is directly used in the 410-460 nm spectral range.

In the second set of experiments, the OH radical products resulting from the unimolecular decay of energized 3-penten-2-one oxide intermediates are detected by UV laser-induced fluorescence (LIF) on the Q<sub>1</sub> and Q<sub>21</sub> lines of the A–X (1,0) transition. The OH radicals are generated upon decay of the CIs in the capillary tube and cooled in the supersonic jet expansion with the remaining Criegee intermediates and other components of the gas mixture.<sup>9-11</sup> In this type of measurement, the UV beam intersects the gas mixture 1 cm downstream from the tip of the capillary in a collision-free region. Here, the UV radiation (~ 1 mJ/pulse) is generated by the frequency-doubled output of a Nd:YAG laser (EKSPLA NL300; 532 nm, 20 Hz) pumped dye laser (ND6000, Rhodamine 590 dye).

### S3. Theoretical Methods

Geometry optimizations and frequency (harmonic or anharmonic) calculations for the ground state and lowest cationic state of the CIs, the torsional barriers connecting *cis* and *trans* conformers of the CIs, and the transition states (TS) associated with the unimolecular H-atom transfer reactions (Scheme S2) were performed at the B2PLYP-D3/cc-pVTZ (VTZ) level of theory using the Gaussian 16 software suite.<sup>12, 13</sup> The B2PLYP-D3/VTZ level of theory is known to work well for obtaining accurate minimum energy and transition state geometries, as well as associated normal mode wavenumbers, for a number of Criegee intermediates.<sup>14, 15</sup> The adiabatic ionization energies (AIE) and vertical ionization energies (VIE) for the eight conformers of 3-penten-2-one oxide are tabulated in Table S3, where the former is the harmonic zero-point energy (ZPE) corrected energy difference between the optimized cation and neutral, and the latter is the electronic energy difference between the cation and the neutral at the optimized neutral ground state geometry. The *cis-trans* torsional barriers in Table S1 also include harmonic ZPE corrections. For the H-atom transfer reactions, single-point energy correction are performed with high-level ab initio calculations using CCSD(T)/aug-cc-pVTZ (AVTZ) and CCSD(T)-F12b/cc-pVTZ-F12 (VTZ-F12) level of theory as implemented in the Molpro package.<sup>16</sup> In addition, anharmonic ZPE corrections from the B2PLYP-D3/VTZ calculations are included for the CIs and the TSs (Table S2).

Vertical electronic excitation energies (VEE) and associated oscillator strengths ( $f$ ) are calculated for each of the conformers of the CIs utilizing complete active space second-order perturbation theory (CASPT2) with the aug-cc-pVDZ (AVDZ) basis set. The CASPT2 computations are based on a the seven-singlet state-averaged complete active space self-consistent field (SA7-CASSCF) reference wavefunction and involve an active space of 12 electrons in 10 orbitals (12,10). Among the ten orbitals, six are occupied and the remaining four are virtual orbitals. The occupied orbitals are three delocalized  $\pi$  orbitals, one 2p orbital localized on the oxygen atoms, and two  $\sigma$  orbitals associated with the carbonyl oxide moiety. The virtual orbitals include two delocalized  $\pi^*$  orbitals, one  $\sigma^*$  orbital localized on the carbonyl oxide functional group, and a diffuse Rydberg orbital, R(3s). A set of selected orbitals relevant to the first  $\pi^* \leftarrow \pi$  transition for the lowest energy conformer of the 3-penten-2-oxide (*tEE*) is shown in Figure S10. In this CASPT2 calculation, an imaginary level shift of 0.4  $E_H$  is used to mitigate the involvement of intruder states. The CASSCF transition dipole moments ( $\mu_{ij}$ ) associated with the electronic transition from the initial (i, ground state in this study) to final (j) electronic states with CASPT2 energies ( $E_{ij}$ ) are used to calculate the oscillator strengths ( $f_{ij}$ ) for the spin-allowed transitions:

$$f_{ij} = \frac{2}{3} E_{ij} \sum_{a=x,y,z} |\mu_{ij}|_a^2$$

UV-vis absorption profiles are simulated for the lowest energy (*tEE*) conformer of 3-penten-2-one oxide using a nuclear ensemble method similar to that described for other Criegee intermediates.<sup>17-19</sup> An

ensemble of 100 initial geometries ( $N_{tot}$ ) for the  $tEE$  conformer is sampled using a Wigner distribution based on the B2PLYP-D3/VTZ optimized geometry and associated normal mode wavenumbers using Newton-X version 2.4.<sup>20, 21</sup> Then, the VEE and  $f$  values accompanying the first  $\pi^* \leftarrow \pi$  transition are calculated for each of the returned geometries using the same CASPT2(12,10)/AVDZ method. An energy-dependent absorption cross-section  $P(E)$  for the  $tEE$  conformer is determined by summing over the 100 Wigner geometries:

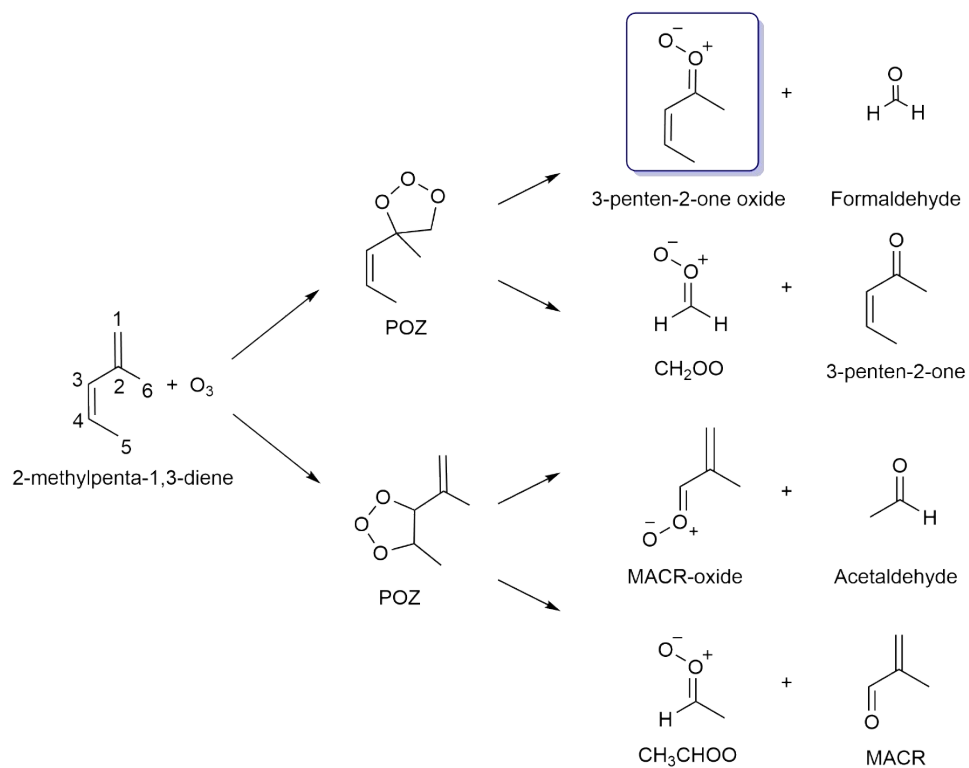
$$P(E) = \frac{\pi e^2}{2m_e c \epsilon_0 N_{tot}} \sum_{N=1}^{N_{tot}} f^N g(E - VEE^N, \delta)$$

where  $m_e$  and  $e$  are the mass and charge of an electron,  $c$  is the speed of light, and  $\epsilon_0$  is the vacuum permittivity. A Lorentzian line shape function ( $g$ ) with a broadening factor  $\delta = 0.3$  eV is assumed for each transition, and  $\hbar$  is the Planck's constant:

$$g(E - VEE^N, \delta) = \frac{\hbar \delta}{2\pi} ((E - VEE^N)^2 + (\frac{\delta}{2})^2)^{-1}$$

All CASSCF and CASPT2 calculations are carried out using the Molpro computation package.<sup>16, 22, 23</sup> In this study, Gaussian and MOLPRO calculations were performed using ACCESS resources.<sup>24</sup>

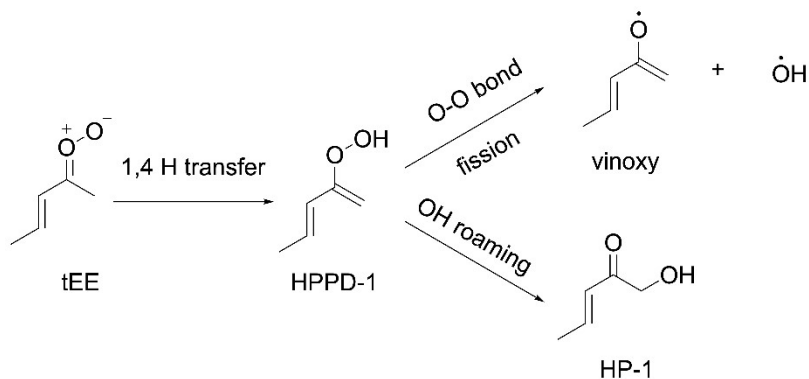
**Scheme S1.** Ozonolysis of 2-methylpenta-1,3-diene proceeds by cycloaddition of ozone across one of the two C=C bonds to form two distinct primary ozonides (POZ). The subsequent decomposition of each POZ can produce two Criegee intermediates and corresponding carbonyl coproducts. Ozonolysis at the C<sub>(1)</sub>=C<sub>(2)</sub> bond of 2-methylpenta-1,3-diene results in a POZ that leads to 3-penten-2-one oxide with formaldehyde or formaldehyde oxide (CH<sub>2</sub>OO) with 3-penten-2-one. Similarly, ozonolysis at the C<sub>(3)</sub>=C<sub>(4)</sub> bond of the parent alkene molecule results in a POZ that leads to methacrolein (MACR)-oxide with acetaldehyde or acetaldehyde oxide (CH<sub>3</sub>CHOO) with MACR. The present study focuses on the 3-penten-2-one-oxide, which is a five-carbon unsaturated Criegee intermediate.



#### S4. Unimolecular Reaction Pathways and Potential Isomers

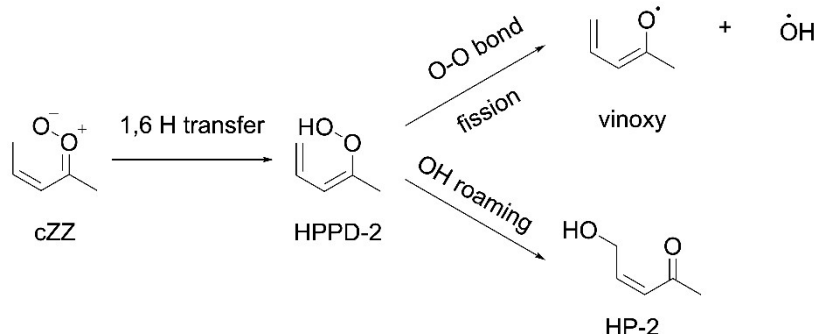
The unimolecular decay pathways for two groups of 3-penten-2-one oxide (first *E* and *Z*) conformers are distinctly different (Figure S9). *E*-conformers have the terminal O-atom pointing toward a methyl group, and thus are expected to undergo unimolecular decay via 1,4 H atom transfer to release OH products.<sup>25</sup> The TS barriers for the 1,4 H-atom transfer mechanism involving a five-membered ring transition state vary from ca. 15.2 to 16.9 kcal mol<sup>-1</sup> for different *E* conformers of 3-penten-2-one oxide (Table S1). As shown in Scheme S2, the lowest energy conformer (*tEE*) may transfer a H-atom to the carbonyl oxide moiety and lead to 2-hydroperoxypenta-1,3-diene (HPPD-1). If subsequent OH roaming occurs, the OH moiety could move to the terminal vinyl site and form a 1-hydroxy-3-penten-2-one (HP-1) isomer.<sup>26, 27</sup>

**Scheme S2.** Unimolecular decay pathways for the *tEE* conformer of 3-penten-2-one oxide Criegee intermediate via a 1,4 H-atom transfer process. The isomeric 2-hydroperoxy-1,3-pentadiene (HPPD-1) is transiently formed, which can subsequently decay to vinyloxy + OH radical products or potentially isomerize to a 1-hydroxy-3-penten-2-one (HP-1) isomer via OH roaming.



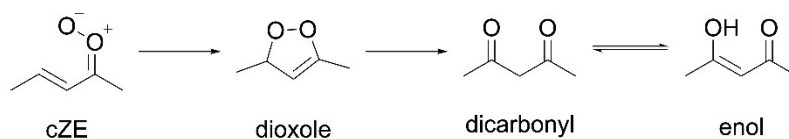
Among the *Z*-conformers, the highest energy *cZZ* conformer has an allylic H-atom, which can migrate to the carbonyl oxide group by an allylic 1,6 H-atom transfer mechanism (Scheme S3) forming a 2-hydroperoxypenta-2,4-diene (HPPD-2) isomer. O-O fission of HPPD-2 can release OH products.<sup>15</sup> Alternatively, if OH roaming occurs, HPPD-2 could also lead to a 5-hydroxy-3-penten-2-one (HP-2) isomer.<sup>26, 27</sup> The allylic 1,6 H-atom transfer is also possible for the *tZZ* conformer via internal rotation about the C-C bond to the *cZZ* conformer with a barrier of ca. 5.5 kcal mol<sup>-1</sup> (Table S1). Compared to 1,4 H-atom transfer, the TS of 1,6 H-atom transfer mechanism involves a seven-membered ring structure with reduced ring strain, significantly reducing the TS barriers to 6.3 and 5.0 kcal mol<sup>-1</sup> for the *tZZ* and *cZZ* conformers, respectively (Table S1).

**Scheme S3.** Unimolecular decay pathways for the *cEE* conformer of 3-penten-2-one oxide Criegee intermediate via a 1,6 H-atom transfer process. 2-hydroperoxy-2,4-pentadiene (HPPD-2) is transiently formed, which can subsequently decay to vinyloxy + OH radical products or possibly isomerize to 5-hydroxy-3-penten-2-one (HP-2) via OH roaming.



The *cZE* conformer has two unsaturated bonds in a *cis* position and a terminal O-atom oriented toward the vinyl substituent. The *cZE* conformer can undergo a 1,5 ring-closure mechanism to form 3,5-dimethyl-3H-dioxole (dioxole). A similar mechanism was demonstrated for *anti-cis* MVK-oxide and *syn-cis* MACR-oxide.<sup>28</sup> The dioxole product can isomerize to 2,4-pentanedione (dicarbonyl) via O-O fission and subsequent 1,2 H-atom transfer. Subsequent tautomerization of this dicarbonyl compound will yield the enolic form (enol). Dioxole, dicarbonyl, and enol are all possible isomers of 3-penten-2-one oxide, as shown in Scheme S4.

**Scheme S4.** Unimolecular decay pathways for the *cZE* conformer of 3-penten-2-one oxide Criegee intermediate via 1,5 ring-closure process. The isomeric 3,5-dimethyl-3H-dioxole (dioxole) is formed, which can subsequently isomerize to 2,4-pentanedione (dicarbonyl). The enolic form (enol) of the dicarbonyl can be formed by tautomerization.



As evident from Table S4, the computed (details of method in Section S3) adiabatic ionization energies of the isomers of 3-penten-2-one oxide indicate that such isomers could contribute to the 10.5 eV photoionization signal on *m/z* 100. However, the computed vertical excitation energies show that their absorption spectra would occur much further into the UV region than the observed spectrum of 3-penten-2-one oxide, and thus would not result in depletion of the photoionization signal in the 320-460 nm region.

## S5. Supplementary Experimental Results

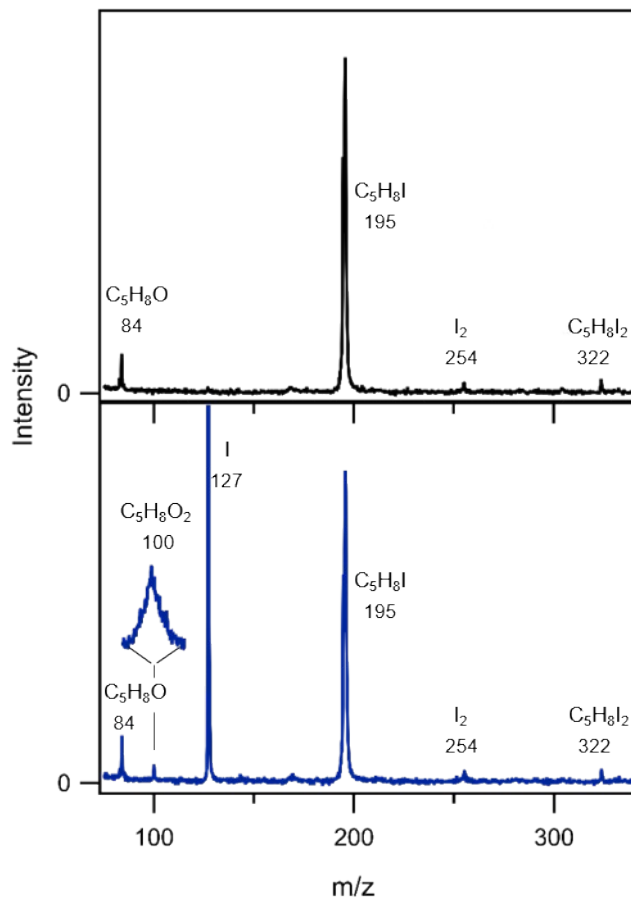


**Figure S7.** The top panel shows the time-of-flight (TOF) mass spectrum of the (*Z*)-2,4-diiodo-pent-2-ene precursor (black trace) recorded upon photoionization at 118 nm (10.5 eV). The precursor was heated to a temperature of 45 °C to increase its vapor pressure. The mass channel at *m/z* 322 corresponds to the precursor (C<sub>5</sub>H<sub>8</sub>I<sub>2</sub>). Additionally, mass channels at *m/z* 254 (I<sub>2</sub>), 195 (C<sub>5</sub>H<sub>8</sub>I), and 84 (C<sub>5</sub>H<sub>8</sub>O) are observed. The bottom panel shows the TOF mass spectrum obtained upon photolysis of the precursor at 248 nm in a 20% O<sub>2</sub>/Ar carrier gas prior to the 118 nm photoionization (blue). The new mass channel at *m/z* 100 corresponds to the 3-penten-2-one oxide Criegee intermediate. The inset displays an expanded view of this mass channel.

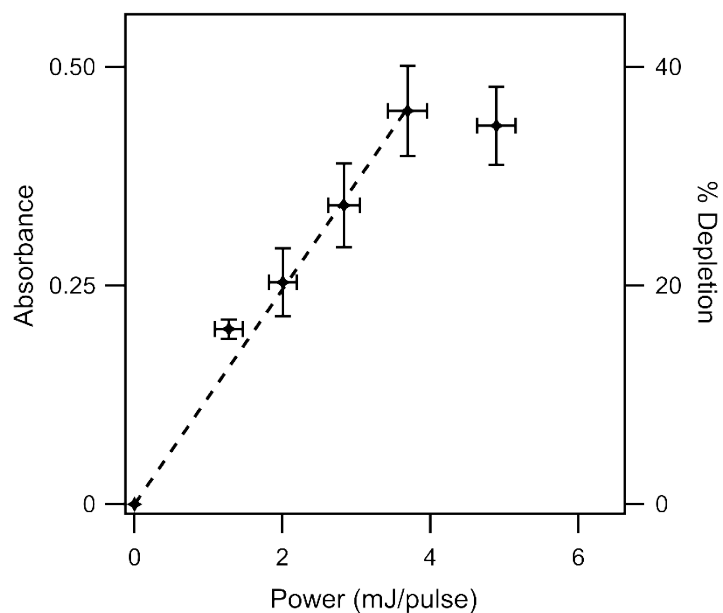


**Figure S8.** Ground state depletion of 3-penten-2-one oxide,  $(N_0 - N)/N_0$ , as a function of OPO power at 410 nm, where  $N$  and  $N_0$  represent the ground state abundance with or without 410 nm excitation. The corresponding absorbance,  $-\ln(N/N_0)$ , exhibits a linear dependence with the OPO power up to ca. 4 mJ/pulse, indicating a one-photon process.

## S6. Supplementary Theoretical Results

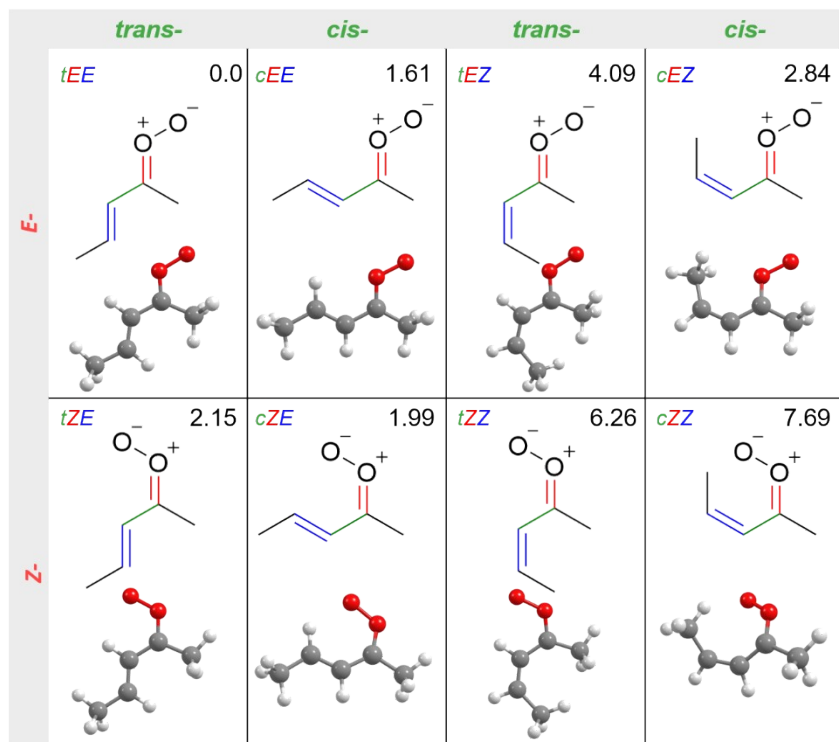


**Figure S9.** Optimized geometries of the eight conformers of the 3-penten-2-one oxide Criegee intermediate. The relative energies are calculated using zero-point energy (ZPE)-corrected CCSD(T)-F12b/VTZ-F12//B2PLYP-D3/VTZ level of theory. High barriers are associated with internal rotation about the C=O bond (red) that connects the *Z* and *E* conformers of the Criegee intermediate. In *E*-conformers, the carbonyl oxide group is directed toward the  $-\text{CH}_3$  group substituent (upper panel), while in *Z*-conformers, it is directed toward the saturated carbon chain (lower panel). Some pairs of *Z/E* conformers are connected by high barriers associated with hindered rotation about the C=C double bond (blue). Furthermore, the *cis* (*c*) and *trans* (*t*) conformers are connected by relatively low barriers associated with internal rotation about the C–C single bond (green).

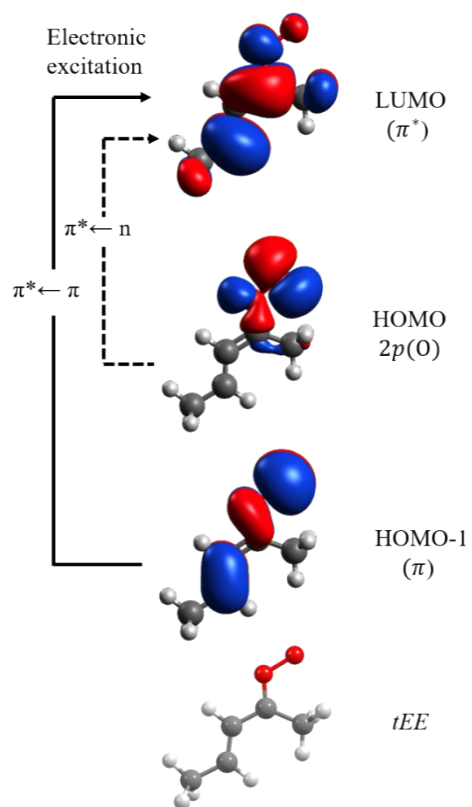


**Figure S10.** Selected orbitals for the lowest energy conformer (*tEE*) of the 3-penten-2-oxide. The arrows represent orbital promotions that occur during the formation of the defined excited states of the CI.

### S6.1. Simulated Absorption Spectra for Additional Low-Energy Conformers

Spectral simulations were performed for the lowest-energy conformer (Figure 2) and four other conformers with energies within 3 kcal mol<sup>-1</sup> (Figure S11) using the nuclear ensemble method as described in Section S3. The spectral simulations for both the lowest-energy conformer (*tEE*, 0 kcal mol<sup>-1</sup>) and the third lowest-energy conformer (*cZE*, 1.99 kcal mol<sup>-1</sup>) are in good agreement with the experimental spectrum with peak at ca. 375 nm and computed absorption cross-sections on the order of 10<sup>-17</sup> cm<sup>2</sup> (Table S5). The lowest *tEE* conformer is predicted to have an even larger absorption cross-section than the *cZE* conformer. Absorption spectra of the other conformers, *cEE* (1.61 kcal mol<sup>-1</sup>), *tZE* (2.15 kcal mol<sup>-1</sup>), and *cEZ* (2.84 kcal mol<sup>-1</sup>), are predicted to peak at longer wavelengths than the experimental spectrum by 20-40 nm (Table S5).

The energized *cZE* conformer can undergo rapid 1,5 ring-closure (Scheme S4, TS of ca. 12 kcal mol<sup>-1</sup>) to yield a dioxole isomer, which is expected to significantly reduce the amount of stabilized *cZE*.<sup>28</sup> The dioxole channel is also accessible for the *tZE* conformer via internal rotation about the C-C bond to form the *cZE* conformer with a barrier of ca. 11 kcal mol<sup>-1</sup> (Table S1). The energized *tEE*, *cEE*, and *cEZ* conformers can undergo 1,4 H-atom transfer reactions with higher TS barriers of ca. 15-17 kcal mol<sup>-1</sup> (Table S2). As a result, the lowest energy *tEE* conformer is likely to be most populated and make the largest contribution to the overall absorption spectrum of 3-penten-2-one oxide.

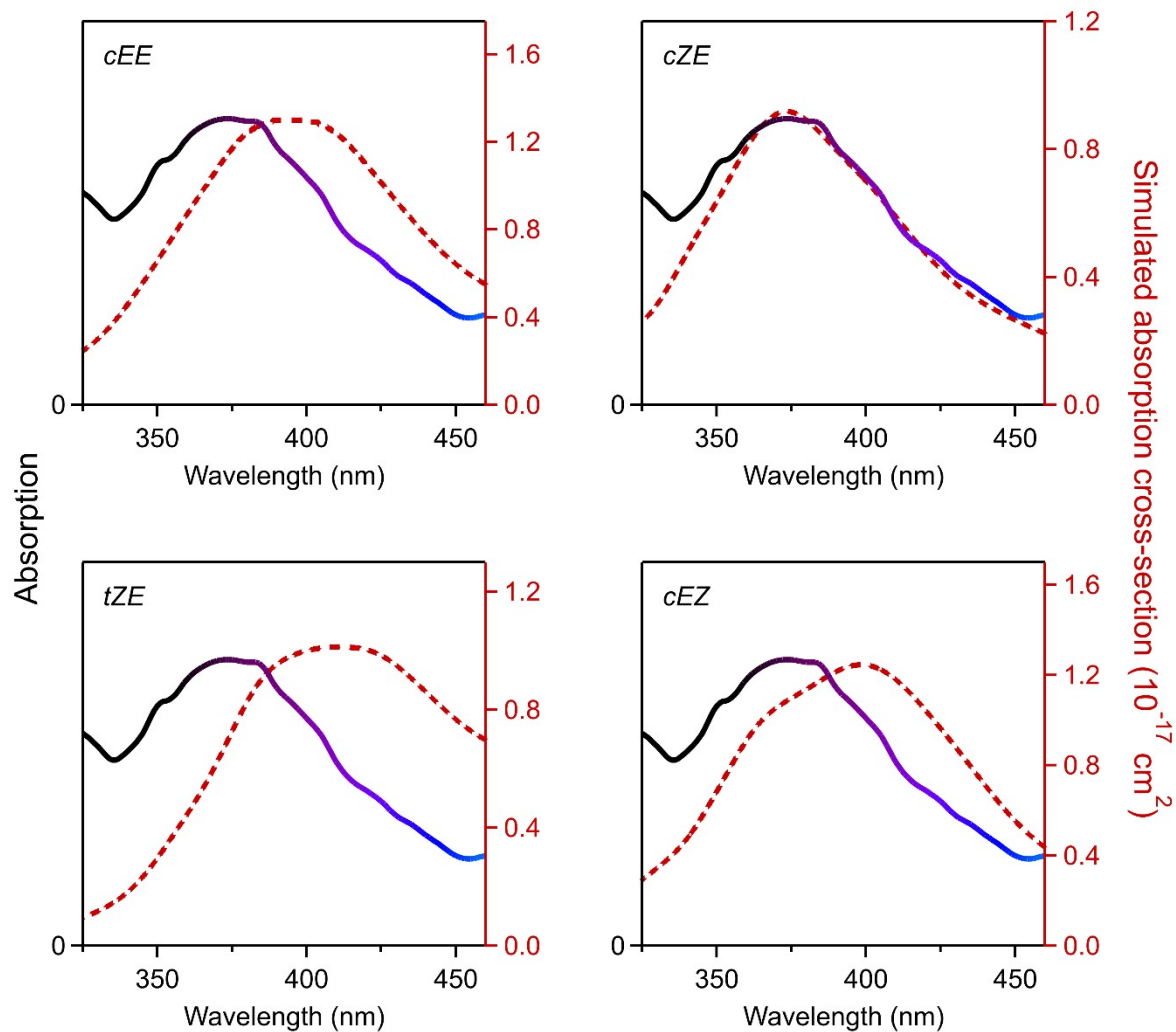


**Figure S11.** In addition to the computed electronic absorption spectrum for the lowest energy *tEE* conformer (Figure 2), spectra have been computed for an additional four low-energy conformers ( $< 3 \text{ kcal mol}^{-1}$ ) of 3-penten-2-one oxide in the 320-460 nm region based on an ensemble of 100 geometries sampled by harmonic-oscillator Wigner distribution of ground state configurations. The simulated first  $\pi^* \leftarrow \pi$  transitions (dashed red) are shown along with the experimentally observed spectrum (solid black to purple).

**Table S1.** Calculated internal rotation barriers for the *cis* to *trans* interconversion of 3-penten-2-one oxide (Figure S9). Energies are harmonic zero-point corrected at B2PLYP-D3/VTZ level of theory.

	B2PLYP-D3/ VTZ (kcal mol <sup>-1</sup> )
<i>cis trans</i> rotation	
<i>cEE</i> to <i>tEE</i>	6.96
<i>cZE</i> to <i>tEZ</i>	5.90
<i>cZE</i> to <i>tZE</i>	10.57
<i>cZZ</i> to <i>tZZ</i>	4.57

**Table S2.** Calculated relative energies using various methods for conformers of 3-penten-2-one oxide and associated transitions states (TS). All energies are zero-point energy (ZPE) corrected and values in parenthesis are corrected with anharmonic ZPE. Figure S9 displays the B2PLYP-D3/VTZ optimized structures.

Species	CCSD(T)/aVTZ// B2PLYP-D3/VTZ (kcal mol <sup>-1</sup> )	CCSD(T)-F12b/VTZ-F12// B2PLYP-D3/VTZ (kcal mol <sup>-1</sup> )
<i>tEE</i>	0.00	0.00
<i>cEE</i>	1.65 (1.69)	1.61 (1.65)
<i>cZE</i>	1.94 (1.63)	1.99 (1.98)
<i>tZE</i>	2.16 (2.15)	2.15 (2.14)
<i>cEZ</i>	2.71 (2.71)	2.84 (2.84)
<i>tEZ</i>	3.93 (3.92)	4.09 (4.07)
<i>tZZ</i>	6.12 (6.12)	6.26 (6.26)
<i>cZZ</i>	7.49 (7.47)	7.69 (7.67)
<u>Effective TS</u>		
Rel. to <i>tEE</i> <sup>a</sup>	16.87 (16.88)	
Rel. to <i>cEE</i> <sup>a</sup>	15.22 (15.19)	
Rel. to <i>cEZ</i> <sup>b</sup>	16.60 (16.61)	
Rel. to <i>tEZ</i> <sup>b</sup>	15.38(15.40)	
Rel. to <i>tZZ</i> <sup>c</sup>	6.34 (6.30)	6.49 (6.45)
Rel. to <i>cZZ</i> <sup>c</sup>	4.97 (4.96)	5.05 5.04)

- tEE* and *cEE* share same TS.
- tEZ* and *cEZ* share same TS.
- tZZ* and *cZZ* share same TS.

**Table S3.** Calculated adiabatic ionization energies (AIE) and vertical ionization energies (VIE) for the eight conformers of 3-penten-2-one oxide (Figure S9) at the B2PLYP-D3/VTZ level of theory. Energies are zero-point energy corrected with harmonic frequencies for AIE.

Conformer	AIE (eV)	VIE (eV)
<i>tEE</i>	7.89	8.04
<i>cZE</i>	8.00	8.18
<i>cEE</i>	7.81	7.99
<i>tZE</i>	7.83	8.00
<i>cEZ</i>	7.91	8.07
<i>tEZ</i>	7.96	8.12
<i>tZZ</i>	7.89	8.05
<i>cZZ</i>	7.95	8.31

**Table S4.** Adiabatic ionization energies (AIE) at B2PLYP-D3/VTZ level of theory, vertical excitation energies (VEE), and corresponding oscillator strengths at CASPT2/AVDZ level of theory for potential isomers (Section S4) of 3-penten2-one oxide.

Isomer	AIE (eV)	VEE (nm)	<i>f</i>
HPPD-1	7.65	208	0.06
HPPD-2	7.49	217	0.25
HP-1	8.79	205	0.04
HP-2	9.07	202	0.25
dioxole	8.10	223	0.06
dicarbonyl	8.90	199	0.02
enol	8.75	264	0.19

**Table S5.** Simulated absorption maxima and associated cross-sections for the low-energy conformers of 3-penten-2-one oxide (<3 kcal mol<sup>-1</sup>).

Conformer	Relative energies (kcal/mol)	Peak position (nm)	Absorption cross-section (10 <sup>-17</sup> cm <sup>2</sup> )
<i>tEE</i>	0.00	376	1.2
<i>cEE</i>	1.65	395	1.3
<i>cZE</i>	1.98	373	0.9
<i>tZE</i>	2.15	411	1.0
<i>cEZ</i>	2.84	398	1.2

**Table S6.** Optimized geometry of each conformer of 3-penten-2-one oxide at the B2PLYP-D3/VTZ level of theory.

<i>tEE</i>			
C	0.00000000	0.00000000	0.00000000
C	0.00000000	0.00000000	1.43432735
O	1.26297958	0.00000000	-1.87352829
C	-1.09772135	0.00000787	2.20777102
O	1.18007996	-0.00000846	-0.52440643
H	-2.07535828	0.00001488	1.74244765
H	0.98231305	-0.00000704	1.89062200
C	-1.15700168	0.00001813	-0.91039940
H	-1.08056330	-0.86592529	-1.57024661
H	-2.10005892	0.00001926	-0.37681971
H	-1.08055003	0.86597271	-1.57023059
C	-1.06981180	0.00000767	3.69793412
H	-1.58812343	0.87493433	4.09429512
H	-1.58813258	-0.87491368	4.09429598
H	-0.05140243	0.00000037	4.07990121
<i>cEE</i>			
C	0.00000000	0.00000000	0.00000000
C	0.00000000	0.00000000	1.44428682
O	1.13676926	0.00000000	-1.95040011
C	1.09379253	0.00000000	2.22249197
O	1.14021437	0.00000000	-0.59202760
H	2.06761932	0.00000000	1.74784517
H	-0.98064428	0.00000000	1.90173964
C	-1.21368349	0.00000000	-0.83464055
H	-1.18396230	-0.86488511	-1.50057256
H	-2.11395305	0.00000000	-0.22911249
H	-1.18396058	0.86488389	-1.50057332
C	1.06247525	0.00000000	3.71105693
H	1.58216177	-0.87438651	4.10699728
H	1.58215822	0.87438749	4.10699756
H	0.04398935	0.00000000	4.09363678
<i>cZE</i>			
C	0.00000000	0.00000000	0.00000000
C	0.00000000	0.00000000	1.42714434
O	2.28558787	0.00000000	-0.21464358
C	1.06773817	0.00000789	2.25607302
O	1.04183958	-0.00000048	-0.75760788
H	2.04952868	0.00001514	1.81203973
H	-0.99306032	-0.00000815	1.86226084

(continued Table S6)

C	-1.28153761	-0.00000064	-0.76710356
H	-1.87562347	-0.87910471	-0.51673136
H	-1.87561449	0.87911328	-0.51674978
H	-1.08019224	-0.00001248	-1.83388222
C	0.93586170	0.00000691	3.73818404
H	1.43580649	-0.87316871	4.16150203
H	1.43577674	0.87320130	4.16149892
H	-0.10282618	-0.00000891	4.06356832
<hr/>			
<i>tZE</i>			
<hr/>			
C	0.00000000	0.00000000	0.00000000
C	0.00000000	0.00000000	1.43049565
O	2.29037229	0.00000000	0.00901140
C	-1.12472160	0.00000000	2.16568660
O	1.11320754	0.00000000	-0.65382008
H	-2.08731208	0.00000000	1.66645518
H	0.98029095	0.00000000	1.88431007
C	-1.21116963	0.00000000	-0.86546031
H	-1.82497992	-0.88014457	-0.67347694
H	-1.82498243	0.88014244	-0.67347433
H	-0.91198422	0.00000000	-1.90939533
C	-1.15099803	0.00000000	3.65465218
H	-1.68551084	0.87466893	4.02985229
H	-1.68550548	-0.87467107	4.02985297
H	-0.14693276	0.00000000	4.07156530
<hr/>			
<i>cEZ</i>			
<hr/>			
C	0.00000000	0.00000000	0.00000000
C	0.00000000	0.00000000	1.43851681
O	1.11953352	0.00000000	-1.96109685
C	1.06675762	0.00050551	2.26291815
O	1.13933345	-0.00007133	-0.60475467
H	0.84897222	0.00036047	3.32300223
H	-0.98644134	-0.00042534	1.87974917
C	-1.21824148	0.00005249	-0.83001072
H	-1.19321117	-0.86497057	-1.49568541
H	-2.11473702	-0.00000104	-0.21911398
H	-1.19324531	0.86519649	-1.49553114
C	2.50638161	0.00121714	1.86588780
H	2.74410260	0.87024852	1.25144402
H	3.15156560	0.00255447	2.73976441
H	2.74540246	-0.86875602	1.25325576

(continued Table S6)

<i>tEZ</i>			
C	0.00000000	0.00000000	0.00000000
C	0.00000000	0.00000000	1.43736956
O	1.30828429	0.00000000	-1.84612029
C	-1.02315115	0.22846294	2.28150683
O	1.19380732	-0.00339532	-0.50316657
H	-0.78588722	0.14296202	3.33452693
H	0.97446734	-0.19733301	1.86511295
C	-1.12759237	-0.06755798	-0.94665141
H	-2.06422743	-0.28998734	-0.45418412
H	-1.19823145	0.86496531	-1.51105839
H	-0.87547058	-0.82620572	-1.69056017
C	-2.43708201	0.61039607	1.97598182
H	-2.53692959	1.14373386	1.03583040
H	-3.08377974	-0.26952321	1.93656371
H	-2.82466651	1.24861716	2.76805982
<i>tZZ</i>			
C	0.00000000	0.00000000	0.00000000
C	0.00000000	0.00000000	1.43183026
O	2.29732910	0.00000000	0.05751652
C	-1.03484605	-0.14964126	2.28066357
O	1.13641276	0.03961973	-0.62398929
H	-0.78480629	-0.07226726	3.33275062
H	0.99252092	0.14633859	1.83396982
C	-1.16132924	0.01493056	-0.93298685
H	-1.69361228	-0.93623783	-0.91460763
H	-1.86730674	0.79997784	-0.66761466
H	-0.80050401	0.18606681	-1.94362266
C	-2.47740066	-0.42292645	2.01568310
H	-2.71354080	-0.58297664	0.97143579
H	-2.79094341	-1.30486806	2.57658279
H	-3.08649662	0.40536966	2.38407240
<i>cZZ</i>			
C	0.00000000	0.00000000	0.00000000
C	0.00000000	0.00000000	1.43801693
O	2.28861538	0.00000000	-0.24221566
C	0.77438505	-0.69768372	2.29426904
O	1.03773365	-0.03032514	-0.76201760
H	0.57296888	-0.52884732	3.34588334
H	-0.81198744	0.57973360	1.86113112
C	-1.27972831	0.13343406	-0.75759087

(continued Table S6)

---

H	-1.94456750	-0.70266326	-0.54255226
H	-1.79619264	1.04577254	-0.45568444
H	-1.08464060	0.17462173	-1.82494306
C	1.78618918	-1.72841214	1.95643195
H	2.42431341	-1.95303184	2.80723729
H	1.28978344	-2.65516326	1.65912097
H	2.37413931	-1.38863512	1.09594334

---

## References

1. S. N. Knezz, T. A. Waltz, B. C. Haenni, N. J. Burrmann and R. J. McMahon, *J. Am. Chem. Soc.*, 2016, **138**, 12596-12604.
2. V. Y. Chen and O. Kwon, *Angew. Chem. Int. Ed.*, 2021, **133**, 8956-8963.
3. J. T. Lowe and J. S. Panek, *Org. Lett.*, 2005, **7**, 1529-1532.
4. J. M. Beames, F. Liu, L. Lu and M. I. Lester, *J. Am. Chem. Soc.*, 2012, **134**, 20045-20048.
5. J. M. Beames, F. Liu, L. Lu and M. I. Lester, *J. Chem. Phys.*, 2013, **138**, 244307.
6. F. Liu, J. M. Beames, A. M. Green and M. I. Lester, *J. Phys. Chem. A*, 2014, **118**, 2298-2306.
7. G. Wang, T. Liu, M. Zou, C. A. Soj dak, M. C. Kozlowski, T. N. V. Karsili and M. I. Lester, *J. Phys. Chem. A*, 2023, **127**, 203-215.
8. F. Liu, J. M. Beames, A. S. Petit, A. B. McCoy and M. I. Lester, *Science*, 2014, **345**, 1596-1598.
9. V. P. Barber, V. J. Esposito, T. Trabelsi, A. S. Hansen, T. A. McHenry, J. S. Francisco and M. I. Lester, *Chem. Phys. Lett.*, 2020, **751**, 137478.
10. G. T. Drozd, T. Kurtén, N. M. Donahue and M. I. Lester, *J. Phys. Chem. A*, 2017, **121**, 6036-6045.
11. V. P. Barber, S. Pandit, V. J. Esposito, A. B. McCoy and M. I. Lester, *J. Phys. Chem. A*, 2019, **123**, 2559-2569.
12. M. J. T. Frisch, G. W.; Schlegel, H. B.; Scuseria, G. E.; and M. A. C. Robb, J. R.; Scalmani, G.; Barone, V.; Petersson, G. A.; Nakatsuji, H.; et al. , **Gaussian 16**, Rev. C.01; Gaussian, Inc.: Wallingford, CT, 2016.
13. S. Grimme, S. Ehrlich and L. Goerigk, *J. Comput. Chem.*, 2011, **32**, 1456-1465.
14. V. P. Barber, A. S. Hansen, Y. Georgievskii, S. J. Klippenstein and M. I. Lester, *J. Chem. Phys.*, 2020, **152**, 094301.
15. A. S. Hansen, Y. Qian, C. A. Soj dak, M. C. Kozlowski, V. J. Esposito, J. S. Francisco, S. J. Klippenstein and M. I. Lester, *J. Am. Chem. Soc.*, 2022, **144**, 5945-5955.
16. H.-J. Werner, P. J. Knowles, F. R. Manby, J. A. Black, K. Doll, A. Heßelmann, D. Kats, A. Köhn, T. Korona, D. A. Kreplin, Q. Ma, T. F. Miller, A. Mitrushchenkov, K. A. Peterson, I. Polyak, G. Rauhut and M. Sibaev, *J. Chem. Phys.*, 2020, **152**, 144107.
17. T. N. V. Karsili, B. Marchetti, M. I. Lester and M. N. R. Ashfold, *Photochem. Photobiol.*, 2023, **99**, 4-18.
18. J. C. McCoy, S. J. Léger, C. F. Frey, M. F. Vansco, B. Marchetti and T. N. V. Karsili, *J. Phys. Chem. A*, 2022, **126**, 485-496.
19. J. C. McCoy, B. Marchetti, M. Thodika and T. N. V. Karsili, *J. Phys. Chem. A*, 2021, **125**, 4089-4097.
20. M. Barbatti, G. Granucci, M. Persico, M. Ruckebauer, M. Vazdar, M. Eckert-Maksić and H. Lischka, *Journal of Photochemistry and Photobiology A: Chemistry*, 2007, **190**, 228-240.
21. M. Barbatti, M. Ruckebauer, F. Plasser, J. Pittner, G. Granucci, M. Persico and H. Lischka, *WIREs Comput. Mol. Sci.*, 2014, **4**, 26-33.
22. H.-J. Werner, P. J. Knowles, G. Knizia, F. R. Manby and M. Schütz, *WIREs Comput. Mol. Sci.*, 2012, **2**, 242-253.
23. H.-J. K. Werner, P. J.; Knizia, G.; Manby, F. R.; Schütz, and P. G. M.; Celani, W.; Kats, D.; Korona, T.; Lindh, R., et al., MOLPRO 2020.1, a package of ab initio programs, see [www.molpro.net](http://www.molpro.net), 2020.
24. J. Towns, T. Cockerill, M. Dahan, I. Foster, K. Gaither, A. Grimshaw, V. Hazlewood, S. Lathrop, D. Lifka, G. D. Peterson, R. Roskies, J. R. Scott and N. Wilkins-Diehr, *Comput. Sci. Eng.*, 2014, **16**, 62-74.
25. V. P. Barber, S. Pandit, A. M. Green, N. Trongsiwat, P. J. Walsh, S. J. Klippenstein and M. I. Lester, *J. Am. Chem. Soc.*, 2022, **140**, 10866-10880.
26. C. A. Taatjes, F. Liu, B. Rotavera, M. Kumar, R. Caravan, D. L. Osborn, W. H. Thompson and M. I. Lester, *J. Phys. Chem. A*, 2017, **121**, 16-23.

27. T. Liu, S. N. Elliot, M. Zou, M. F. Vansco, C. A. Sojda, C. R. Markus, R. Almeida, K. Au, L. Sheps, D. L. Osborn, C. J. Percival, C. A. Taatjes, R. L. Caravan, S. J. Klippenstein, M. I. Lester, *J. Am. Chem. Soc.*, 2023, <https://doi.org/10.1021/jacs.3c07126>.
28. M. F. Vansco, R. L. Caravan, K. Zuraski, F. A. F. Winiberg, K. Au, N. Trongsirawat, P. J. Walsh, D. L. Osborn, C. J. Percival, M. A. H. Khan, D. E. Shallcross, C. A. Taatjes and M. I. Lester, *J. Phys. Chem. A*, 2020, **124**, 3542-3554.